Synthesis and Characterization of Poly(isobenzofuran) Films by Chemical Vapor Deposition

Hyun-Goo Choi,[†] John P. Amara,[‡] Timothy M. Swager,[‡] and Klavs F. Jensen*[,†]

Department of Chemical Engineering and Department of Chemistry, Massachusetts Institute of Technology, 77 Massachusetts Avenue, Cambridge, Massachusetts 02139

Received February 15, 2006; Revised Manuscript Received April 13, 2006

ABSTRACT: This paper describes the synthesis and properties of poly(isobenzofuran) (PIBF) films prepared by a thermal chemical vapor deposition (CVD) process. The synthesized precursor monomer, 1,2,3,4-tetrahydro-1,4-epoxynaphthalene, is pyrolyzed by flowing it through a tube furnace at temperatures of 600−750 °C. A reactive intermediate, isobenzofuran (IBF) monomer, is produced by this pyrolysis and deposited onto a silicon substrate where it polymerizes to form a thin coating of poly(isobenzofuran) (PIBF) on the surface. The chemical structure and composition of the PIBF films are supported by nuclear magnetic resonance (NMR) spectroscopy, Fourier transform infrared spectroscopy (FT-IR), and X-ray photoelectron spectroscopy (XPS). The weight-average molecular weight of the PIBF films range from 5500 to 9400 by varying the deposition (stage), pyrolysis (furnace), and vaporization (source) temperatures. With the variation of deposition temperature (5, 10, 15, 20, 25 °C) and pyrolysis temperature (600, 650, 700, 750 °C), significant changes are observed in deposition (growth) rate, molecular weight, and morphology while the chemical structure of the PIBF films remain the same as probed by FT-IR and XPS analysis. On the other hand, variation of the vaporization temperature (40, 45, 50, 55, 60 °C) leads to significant changes in the chemical structure as well as in the deposition rate, molecular weight, film uniformity, and morphology. By exploring several operating conditions, we have obtained optimal conditions for deposition temperature (10 °C), pyrolysis temperature (750 °C), and vaporization temperature (60 °C) that provide good film properties as well as fast film growth. To investigate the possible role of cationic initiation in IBF polymerization, PIBF films were deposited on several surfaces tailored with self-assembled monolayers (SAMs) of thiols that have functional groups of different acidities, including a carboxylic acid (−COOH), a phenol (−PhOH), an alcohol (−OH), an amine ($-NH_2$), and a methyl group ($-CH_3$). We observed the fastest growth of PIBF ($k = 2.5$ Å/s) on the carboxylic acid-terminated surfaces whereas the slowest growth was on the methyl-terminated surfaces ($k = 0.02$ Å/s). On the basis of the experimental observations, we proposed a growth mechanism for the PIBF films by the CVD process.

Introduction

Among the many techniques for the preparation of polymeric thin films, the chemical vapor deposition (CVD) process is a promising method to provide functional polymer coatings. CVD processes have several advantages, including pinhole-free, solvent-free, and noncontact deposition of uniform coatings for complex structures, compared to conventional liquid-phase processing methods, such as dip coating, spin coating, and roll coating, etc. Among the widely studied class of polymer coatings by CVD is poly(*p*-xylylene) (PPX, commercially known as parylene) and its derivatives, which are used for low dielectric coatings,[1] corrosion-resistant coatings,[2] biopassivation layers,[3] as components of microelectromechanical systems (MEMS) such as membranes and channel walls,[4] waveguides and coatings for optical systems,[5] patterned surfaces,[6] and reactive coatings in biological applications.[7] Fluorocarbon films constitute another extensively studied class of polymer CVD coatings for the development of low dielectric materials and as water-repellent coatings (hydrophobic surfaces).[8] Additional examples of polymer CVD coatings include conjugated polymers, such as poly(*p*-phenylenevinylene) (PPV) for electroluminescent materials,[9] poly(pyrrole) and poly(thiophene) for conductive layers and photovoltaic devices,[10] and poly(2,4-hexadiyn-1,6-diol) (PHDO) for highly conductive materials.[11] The preparation of fluorocarbon/organosilicon copolymer films and poly(ethylene glycol) (PEG) films by CVD processes have also been investigated for biological applications.[12]

Scheme 1. Formation and Polymerization of Isobenzofuran (IBF)

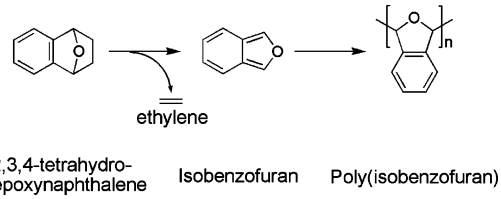

Isobenzofuran (IBF) is a highly reactive molecule and is often generated in synthetic pathways in-situ as a reactive intermediate. The high reactivity of IBF under ambient conditions can provide access to a variety of naphthalenes and heterocyclic derivatives.[13] Since IBF was isolated and characterized by Fieser and Haddadin in 1964,[14] there has been considerable interest in the synthetic utility of this transient intermediate. IBF has been generated by retro-Diels−Alder fragmentation of 1,4-dihydro-1,4-endooxynaphthalene,[14] a controlled pyrolysis (120 °C and 0.1 Torr) of the adduct of 1,4-dihydro-1,4-endooxynaphthalene and 3,6-di(2-pyridyl)-*s*-tetrazine followed by a cold trapping (at −80 °C),[15] and a flash vacuum thermolysis (650 °C and 0.1 Torr) of 1,2,3,4-tetrahydro-1,4-epoxynaphthalene followed by a cold trapping.[16] IBF can be isolated at low temperature, but under ambient conditions its high reactivity leads to further reactions such as polymerization, as shown in Scheme 1.[13−16] Although the polymerization of IBF has been briefly mentioned in early reports of the chemistry of IBF, to

* To whom correspondence should be addressed. E-mail: kfjensen@mit.edu; Fax: (617) 258-8224.
[†] Department of Chemical Engineering.
[‡] Department of Chemistry.

10.1021/ma060345n CCC: $33.50
Published on Web 06/03/2006

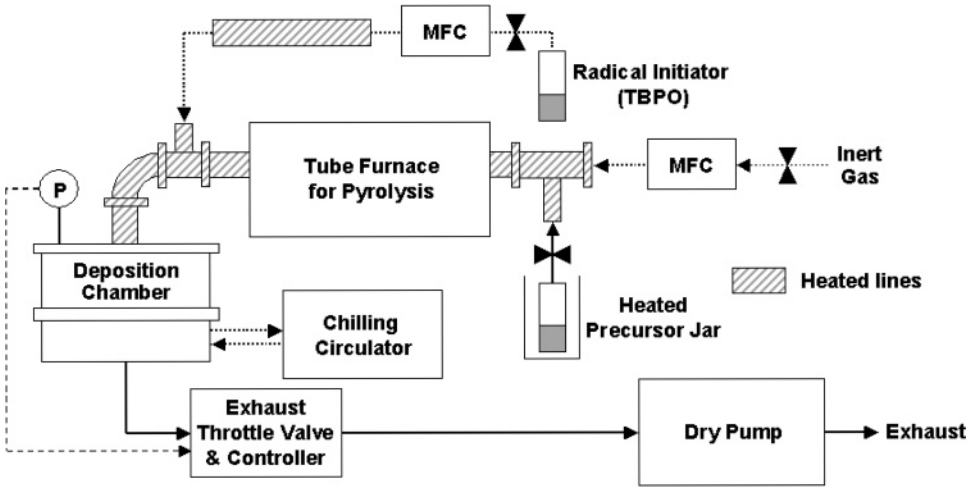

Figure 1. Diagram of the CVD reactor used for polymerization of IBF. The initiator (*tert*-butyl peroxide, TBPO) was used only for the investigation of a possible radical initiation of IBF polymerization. Inert gas (argon) was used only for purging of feed line before each batch.

our knowledge, a polymeric form of IBF has never been intentionally synthesized, isolated, or characterized.

Herein we present the polymerization of IBF by a CVD process. The poly(isobenzofuran) (PIBF) films were prepared under various operating conditions and characterized as a function of deposition (stage) temperature, pyrolysis temperature, and vaporization (source) temperature by Fourier transform infrared (FT-IR) spectroscopy, X-ray photoelectron spectroscopy (XPS), gel permeation chromatography (GPC), ellipsometry, and microscopy techniques. The growth of PIBF films on several surfaces with functional groups of different acidities was also performed to investigate a possible role of cationic initiation of IBF polymerization. The observations provide insight into the polymerization mechanism of IBF and the optimal conditions for IBF polymerization by CVD.

Experimental Section

Materials. A precursor monomer, 1,2,3,4-tetrahydro-1,4-epoxynaphthalene, was either obtained from Acros Organics (Morris Plains, NJ) or synthesized according to the described synthetic procedure.[17] Silicon wafers (p-type, 100) were purchased from Montco Silicon Technologies, Inc. (Spring City, PA). Other materials and reagents were purchased from Aldrich (Milwaukee, WI). All chemicals were of reagent grade and used as received.

Polymerization of Isobenzofuran (IBF) by Chemical Vapor Deposition (CVD). Polymerization of IBF was performed by cracking 1,2,3,4-tetrahydro-1,4-epoxynaphthalene in a home-built CVD system. As shown in Figure 1, the thermal CVD system was composed of a monomer delivery (vaporization) zone, pyrolysis zone, and deposition zone. The precursor monomer was placed in a glass jar heated to 40−60 °C, and the vapor was flowed through a 1 in. diameter quartz tube in a Lindberg tube furnace (Watertown, WI) where the pyrolysis temperature was controlled to 600−850 °C. Reactive intermediate species, IBF monomer, was produced by pyrolysis and flown to the deposition chamber (10 in. diameter and 5 in. height) through a heated line ($T \geq 100$ °C). The line was heated to minimize polymer deposition on the walls of transport zone. Ethylene gas, produced as a pyrolysis byproduct shown in Scheme 1, was vented to the exhaust. The pressure within the chamber was controlled at 0.2 Torr by an exhaust valve (Type-253, MKS Instruments, Andover, MA) connected to an exhaust valve controller (Type-252, MKS Instruments, Andover, MA). The stage temperature of deposition chamber was controlled to 5−25 °C by circulating chilled water through internal coils on the backside of the deposition surface (stage).

For the investigation on the possibility of cationic initiation of IBF polymerization, deposition of PIBF on several surfaces tailored with functional groups of different acidities was performed under similar conditions. Surfaces with different functional groups were prepared by forming self-assembled monolayers (SAMs) of thiols on gold surbstrates. Polycrystalline gold films were prepared by sequential electron beam evaporation of Ti (5 nm) and Au (30 nm) on silicon substrates. Gold-coated silicon substrates were then soaked into 2 mM ethanolic solutions of 11-mercaptoundecanoic acid, 4-mercaptophenol, 11-mercapto-1-undecanol, 2-aminoethanethiol hydrochloride, and 1-undecanethiols for 18 h. The modified gold substrates were then removed from the solution and dried under a stream of nitrogen prior to use.

To investigate the possibility of radical initiation of IBF polymerization, deposition of PIBF was performed with *tert*-butyl peroxide (TBPO) as a radical initiator.[18] TBPO was vaporized in a glass jar at room temperature and fed to a deposition chamber through a mass flow controller (model 1479A, MKS Instruments, Andover, MA). The feed line between the mass flow controller and the deposition chamber was heated to 220 °C to produce radical initiators by thermal cracking of TBPO. Reactive intermediate and radical initiator (TBPO) were mixed together before entering the deposition chamber. The flow rate of precursor monomer was kept at 2.0 sccm whereas that of TBPO was varied (i.e., 0, 0.2, 0.4, and 0.8 sccm).

Characterization of Poly(isobenzofuran) (PIBF) Films. Film thickness was measured by variable angle spectroscopic ellipsometry (VASE) with a J.A. Woollam M-2000s rotating compensator ellipsometer (J.A. Woollam Co., Inc., Lincoln, NE). For each film, ellipsometric psi (Ψ) and delta (Δ) angles were measured over the wavelength from 315 to 800 nm, at three incident angles of 65°, 70°, and 75°. A subsequent regression methodology was used to derive thickness and optical properties of the films according to the literature.[19] With an automated sample translator, the thickness and refractive index were measured on 73 points over the substrate, and the thickness profiles of each film were obtained by mapping the data. The deposition was monitored in-situ by interferometry using 632.8 nm He−Ne laser light (JDS Uniphase, San Jose, CA). A cycle thickness was calculated by dividing the total thickness of films by the number of cycles. Fourier transform infrared (FT-IR) spectra were obtained with a Nicolet Nexus 870 spectrometer (Thermo Nicolet Corp., Madison, WI) in normal transmission mode using a deuterated triglysine sulfate (DTGS) KBr detector over the range 400−4000 cm^{-1} at 4 cm^{-1} resolution. X-ray photoelectron spectroscopy (XPS) was used to monitor the surface composition of PIBF films. XPS spectra were obtained with a Kratos Axis Ultra spectrometer (Kratos Analytical, Chestnut Ridge, NY) equipped with a monochromatized Al Kα X-ray source. Pass energies were 160 and 10 eV for survey and high-resolution scans, respectively. All peaks were fitted with 100% Gaussian, and the peak positions

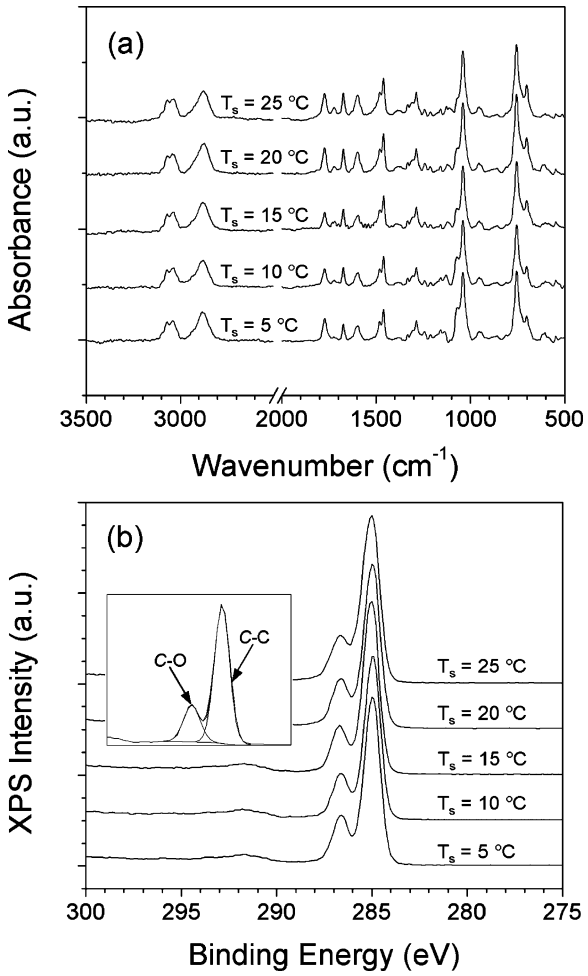

Figure 2. (a) FT-IR spectra of PIBF films prepared at various stage temperatures. (b) C(1s) high-resolution XPS spectra of the PIBF films prepared at various stage temperatures. The inset is a typical example of the curve fitting for the two peak components (i.e., *C*−C and *C*−O centered at 285.0 and 286.7 eV, respectively). Other operating conditions were fixed at T_p = 750 °C, T_v = 60 °C, and P = 0.2 Torr.

were referenced to C(1s) = 285.0 eV. Nuclear magnetic resonance (NMR) spectra were obtained on a Varian Inova 500-MHz spectrometer. All polymer solutions were filtered through 0.45 μm syringe filters prior to use, and the NMR chemical shifts were referenced to $CDCl_3$/TMS (7.27 ppm for ^{1}H and 77.23 ppm for ^{13}C). The molecular weight of the PIBF film was measured by gel permeation chromatography (GPC) with a Waters 1525 binary high-performance liquid chromatography (HPLC) pump (Waters, Milford, MA) equipped with a R410 differential refractometer as a detector. All polymer films were dissolved in tetrahydrofuran (THF) and filtered prior to use. Polystyrene standards from Aldrich were used for calibration, and THF was used as an eluent. Optical microscopy images were obtained with an optical microscope (Nikon, TE300) equipped with a digital camera and image processing software. Electron micrographs were taken on a scanning electron microscope (JEOL, JSM5910) with a spot size of 44 μm and acceleration voltage of 2.0 kV. Surface morphologies were analyzed with a NanoScope III atomic force microscope (Digital Instruments) operating in a tapping mode. Stress measurements on PIBF films were performed with a Tencor flexus FLX-2320 stress gauge (KLA Tencor) by analyzing the difference in curvature between a bare silicon substrate and a PIBF film deposited silicon substrate.

Results and Discussion

Deposition (Stage) Temperature Dependence of PIBF Film Growth. Figure 2a shows the FT-IR spectra of the PIBF films prepared by varying the deposition (stage) temperatures (T_s) from 5 to 25 °C with an interval of 5 °C while other conditions were fixed (T_p = 750 °C, T_v = 60 °C, and P = 0.2 Torr, where subscripts p and v represent pyrolysis and vaporization, respectively). We observed that all FT-IR spectra in this set of PIBF films exhibit nearly identical absorption bands, and all of the bands can be clearly resolved.[20] The sp^2 C−H stretch from benzene ring is observed at 3040 cm^{-1}, and the sp^3 C−H stretch from the polymer backbone is also detected at 2874 cm^{-1}. The C═C aromatic stretch absorptions are observed in a pair at 1595 and 1460 cm^{-1}. The furanoid C−O stretch absorptions are also detected in a pair at 1285 and 1038 cm^{-1}. Furthermore, other absorptions, such as weak combination/overtone bands for the ortho-substituted (1670−1900 cm^{-1}) and out-of-plane bending vibration for the ortho-substituted (755 cm^{-1}), provide useful insights into the chemical structure of the PIBF polymer.

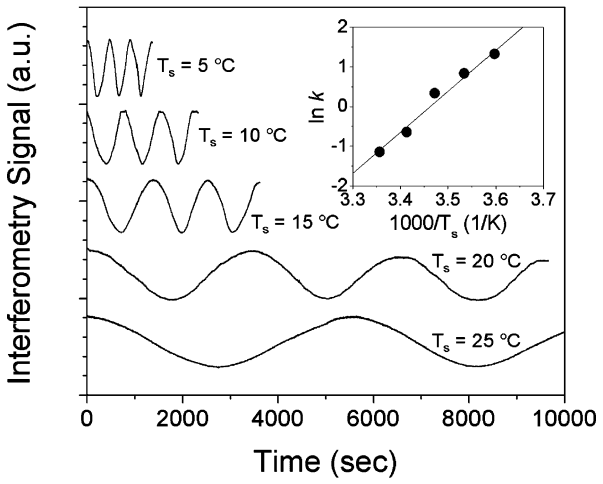

Figure 3. Interferograms obtained during the PIBF film growth at different stage temperatures using a 632.8 nm He−Ne laser. Other operating conditions were fixed at T_p = 750 °C, T_v = 60 °C, and P = 0.2 Torr. The inset is a kinetic analysis of PIBF film growth as a function of the stage (surface) temperature.

The atomic composition of PIBF films was confirmed by XPS. Survey scans revealed the typical atomic composition of the PIBF films as 84.8% (C) and 15.2% (O), consistent with the stoichiometriy of PIBF (85.7% of carbon and 14.3% of oxygen). To verify the PIBF structure, we also performed high-resolution scans on this set of PIBF films (Figure 2b). Each spectrum consists of two peak components corresponding to the unsaturated carbons (i.e., *C*−C or *C*−H in the benzene ring) and the oxygen-bound carbon (i.e., *C*−O in the furanoid ring), centered at the binding energies of 285.0 and 286.7 eV, respectively. Area fractions of these peak components are typically 75.9% (*C*−C or *C*−H) and 24.1% (*C*−O), in good agreement with the stoichiometry of PIBF (75% of *C*−C and 25% of *C*−O). The results from FT-IR and XPS analysis suggest that the PIBF films obtained with various stage temperatures are nearly identical with one another in terms of the chemical structure and the atomic composition of the films.

By using interferometry (Figure 3), the deposition (growth) kinetics of PIBF films was explored as a function of the stage temperature, T_s. The deposition rate decreases as the stage temperature increases. At T_s = 5 °C, it takes about 22 min to obtain a 0.5 μm thick film (deposition rate, k = 3.8 Å/s), whereas more than 4.5 h is needed to obtain a similar film thickness (k = 0.32 Å/s) at T_s = 25 °C. A semilogarithmic plot of growth rate against the reciprocal stage temperature (inset of Figure 3) yields a slope of 10325 K (and hence ΔE_a = −85.9 kJ/mol) and an intercept of k_0 = 0.186 Å/s. The decreasing

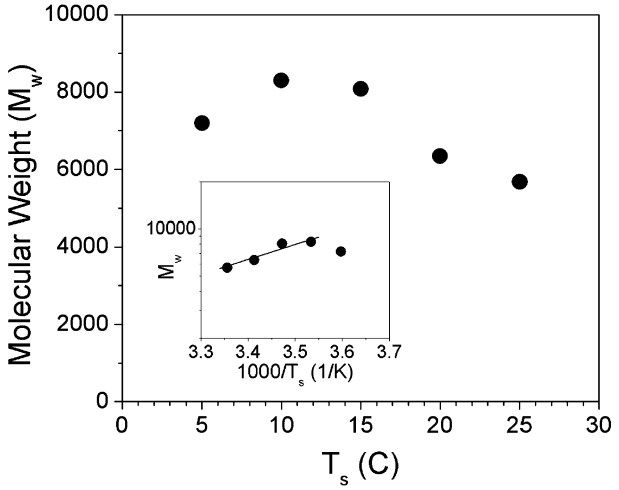

Figure 4. Weight-average molecular weight (M_w) of PIBF films as a function of the stage temperature. Other operating conditions were fixed at $T_p = 750$ °C, $T_v = 60$ °C, and $P = 0.2$ Torr.

growth rate with increasing temperature can be interpreted in terms of competition between surface adsorption and desorption. In this simple model, reactive intermediates adsorb on the surface and then either desorb or form polymer. The rates of adsorption and desorption have the following dependence on stage (deposition) temperature (T_s):

$$r_{ads} \propto \exp\left(-\frac{E_a^{ads}}{RT_s}\right) \quad \text{and} \quad r_{des} \propto \exp\left(-\frac{E_a^{des}}{RT_s}\right) \qquad (1)$$

The highly reactive monomer species formed in the pyrolysis would be expected to have a very low activation barrier for adsorption (i.e., $E_a^{ads} \sim 0$ and thereby $\Delta E_a = (E_a^{des} - E_a^{ads}) \sim E_a^{des}$). As a result, the growth rate would be expected to vary as

$$r_{growth} \propto \frac{r_{ads}}{r_{des}} \exp\left(-\frac{E_a^{des}}{RT_s}\right) \qquad (2)$$

and hence it will decrease as the stage temperature increases.

As the stage temperature is increased from 5 to 25 °C, the weight-average molecular weight of the PIBF film reaches a maximum of 8300 at 10 °C and then decreases to 5600 at 25 °C (Figure 4). These changes in molecular weight with the variation of the stage temperature are consistent with the polymerization of IBF, primarily controlled by a surface growth mechanism. The adsorption efficiency of the IBF monomer at $T_s = 5$ °C is better than that at $T_s = 10$ °C. Accordingly, there would be more nucleation sites for polymerization (i.e., growing polymer chains) over the entire surface at $T_s = 5$ °C than that present at $T_s = 10$ °C, leading to a large number of polymer chains with lower molecular weight. The increase in desorption rate with stage temperature leads to the reduction of residence time of IBF monomer on the surface with a corresponding reduction in the rate of initiation and propagation of polymerization and reduction in the molecular weight of the PIBF films.

Figure 5 shows the uniformity of the PIBF films at the typical growth conditions. The thickness of the PIBF film is 510 and 400 nm at the center and the edge of the substrate, respectively.[21] The films prepared at $T_s = 5$, 10, and 15 °C show similar trends, but the film uniformity deteriorates with further increases in the stage temperature. The standard deviations of thickness obtained from the films prepared at $T_s = 5$, 10, and 15 °C are almost the same, ~53 ± 1 nm, while larger standard deviations are observed in the films prepared at $T_s = 20$ and 25 °C (57 and 65 nm, respectively). Since the IBF monomer is delivered from the top-center part of the reactor to the center of the substrate, the IBF molecules accumulate near the center region and then diffuse to the edge. This process sets up a concentration gradient of the IBF monomers with a maximum at the center of the substrate and decreasing along with the radial direction of the substrate. Correspondingly, the polymer films grow thicker at the center than on the edge of the substrate. By considering the deposition rate, the molecular weight, and the film uniformity, we selected 10 °C as an optimal stage temperature for the PIBF film growth.

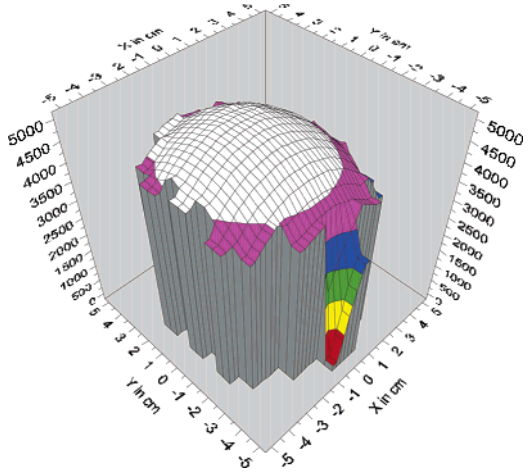

Figure 5. Thickness profile of PIBF film prepared at $T_s = 10$ °C, $T_p = 750$ °C, $T_v = 60$ °C, and $P = 0.2$ Torr.

Pyrolysis Temperature Dependence of PIBF Film Growth. Figure 6a shows the FT-IR spectra in the PIBF films prepared at the various pyrolysis temperatures (T_p, from 600 to 750 °C with an interval of 50 °C) while other conditions were fixed ($T_s = 10$ °C, $T_v = 60$ °C, and $P = 0.2$ Torr, where subscripts s and v represent stage and vaporization, respectively). We observed no significant differences in the FT-IR spectra of this set of PIBF films. All spectra are nearly identical to one another and also have the same absorption bands that were present in the spectra of the PIBF films prepared at the different stage temperatures (Figure 2a).

The atomic composition of the PIBF films was confirmed by XPS. From survey scans, the typical atomic composition of this set of PIBF films was 84.9% (C) and 15.1% (O), consistent with those from the various stage temperatures and the stoichiometry of PIBF (85.7% of carbon and 14.3% of oxygen). High-resolution scans (Figure 6b) exhibit nearly identical features in the C(1s) region as observed from the films with the stage temperature variations. Each spectrum consists of two peak components corresponding to the unsaturated carbons (i.e., *C*−C or *C*−H in the benzene ring) and the oxygen-bound carbon (i.e., *C*−O in the furanoid ring), centered at the binding energies of 285.0 and 286.7 eV, respectively. Area fractions of these peak components are typically 75.7% (*C*−C or *C*−H) and 24.3% (*C*−O), in good agreement with the stoichiometry of PIBF (75% of *C*−C and 25% of *C*−O).

We analyzed the deposition rate of the PIBF films as a function of the pyrolysis temperature, T_p. The deposition rate is reduced as the pyrolysis temperature decreases. At $T_p = 750$ °C, it takes about 36 min to obtain a 0.5 μm thick film (deposition rate, $k = 2.3$ Å/s), whereas more than 9 h is required to obtain a similar film thickness ($k = 0.16$ Å/s) with $T_p = 600$ °C (interferograms not shown). We plotted the deposition rate of each film against the pyrolysis temperature in an Arrhenius form as shown in Figure 7 and obtained the apparent activation

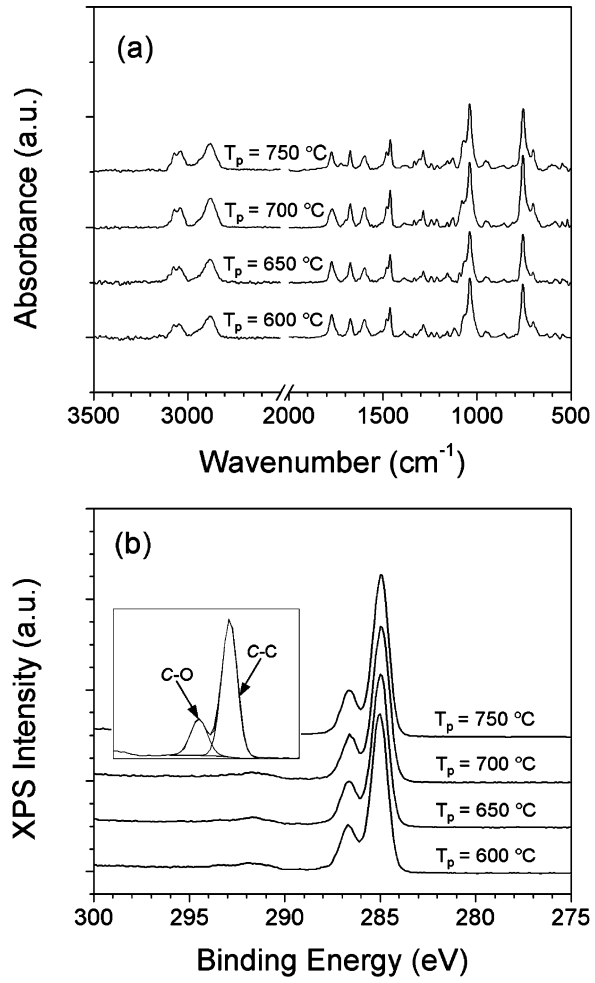

Figure 6. (a) FT-IR spectra of PIBF films prepared at various pyrolysis temperatures. (b) C(1s) high-resolution XPS spectra of the PIBF films prepared at various pyrolysis temperatures. The inset is a typical example of the curve fitting for two peak components (i.e., *C*−C and *C*−O centered at 285.0 and 286.7 eV, respectively). Other operating conditions were fixed at T_s = 10 °C, T_v = 60 °C, and P = 0.2 Torr.

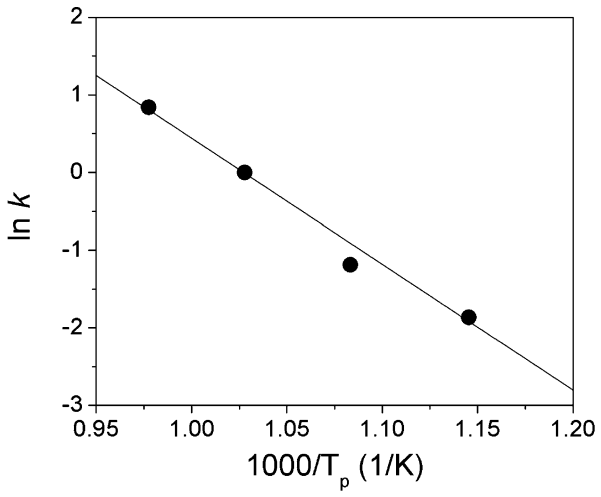

Figure 7. Deposition (growth) kinetics of the PIBF films prepared at various pyrolysis temperatures. Other operating conditions were fixed at T_s = 10 °C, T_v = 60 °C, and P = 0.2 Torr. An apparent activation energy and a frequency factor can be calculated from the line fitting (i.e., $\ln k = \ln k_0 - E_a^p/RT_p$).

energy for pyrolysis (E_a^p = 134.7 kJ/mol) with a frequency factor (k_0 = 0.287 Å/s). The polymerization of IBF can be considered as a self-initiated process, where the pyrolysis of the precursor monomer (1,2,3,4-tetrahydro-1,4-epoxynaphthalene) is the critical step to generate the IBF monomer and governs the overall polymerization reaction. The cracking efficiency of the precursor monomer increases with pyrolysis temperature, and as a result, the amount of IBF monomer and the rate of initiation of polymerization increase accordingly.

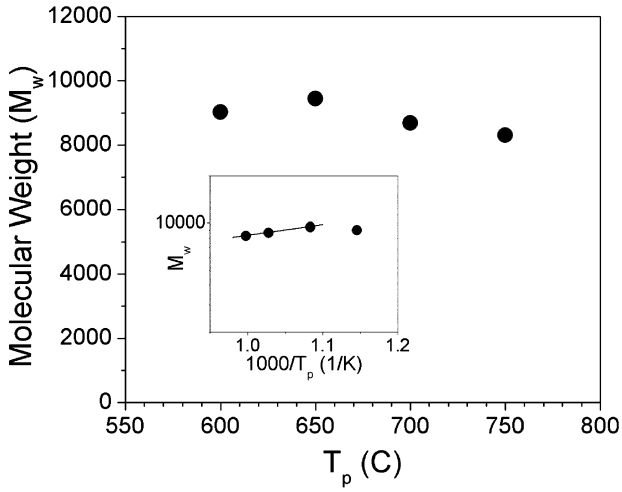

Figure 8. Weight-average molecular weight of PIBF films as a function of the pyrolysis temperature. Other operating conditions were fixed at T_s = 10 °C, T_v = 60 °C, and P = 0.2 Torr.

The molecular weight of this set of PIBF films (Figure 8) shows little variation, ranging from 8300 to 9400, with a slight decrease as the pyrolysis temperature increases. This slight decrease in the molecular weight could be attributed to a large number of IBF monomers produced at higher pyrolysis temperature, leading to more growing polymer chains (i.e., more propagation centers). However, it seems that there is no dependence of molecular weight on the pyrolysis temperature in this range because the standard deviation of the molecular weight for this series of PIBF films is 500, which falls into the acceptable error range of the measured values. We selected 750 °C as an optimal pyrolysis temperature for the PIBF film growth by considering the deposition rate, the molecular weight, and the film uniformity.[22]

Vaporization (Source) Temperature Dependence of PIBF Film Growth. Unlike the PIBF films prepared at the various stage temperatures and the various pyrolysis temperatures, the PIBF films prepared at the various vaporization (source) temperatures exhibit remarkable differences in the chemical structure, molecular weight, and film uniformity. Figure 9a shows the FT-IR spectra of the PIBF films prepared at the various vaporization temperatures (T_v, from 40 to 60 °C with an interval of 5 °C) while other conditions were fixed (T_s = 10 °C, T_p = 750 °C, and P = 0.2 Torr, where subscripts s and p represent stage and pyrolysis, respectively). We observed that the sp^2 C−H stretch from the benzene ring (3040 cm^{-1}) and the sp^3 C−H stretch from the polymer backbone (2874 cm^{-1}) decrease as the vaporization temperature decreases. Especially, the sp^3 C−H stretch from the polymer backbone (2874 cm^{-1}) disappeared from the spectrum of the PIBF film prepared at T_v = 40 °C. We also recognized that other absorptions, such as the C═C aromatic stretch (a pair at 1595 and 1460 cm^{-1}) and the furanoid C−O stretch (a pair at 1285 and 1038 cm^{-1}), show reduction in intensity and shifts in peak position. The reduction in the peak intensity and shift in peak position of several absorptions indicate the decrease in the degree of polymerization and the generation of different organic frameworks with small molecular weight through a different pathway; this result is

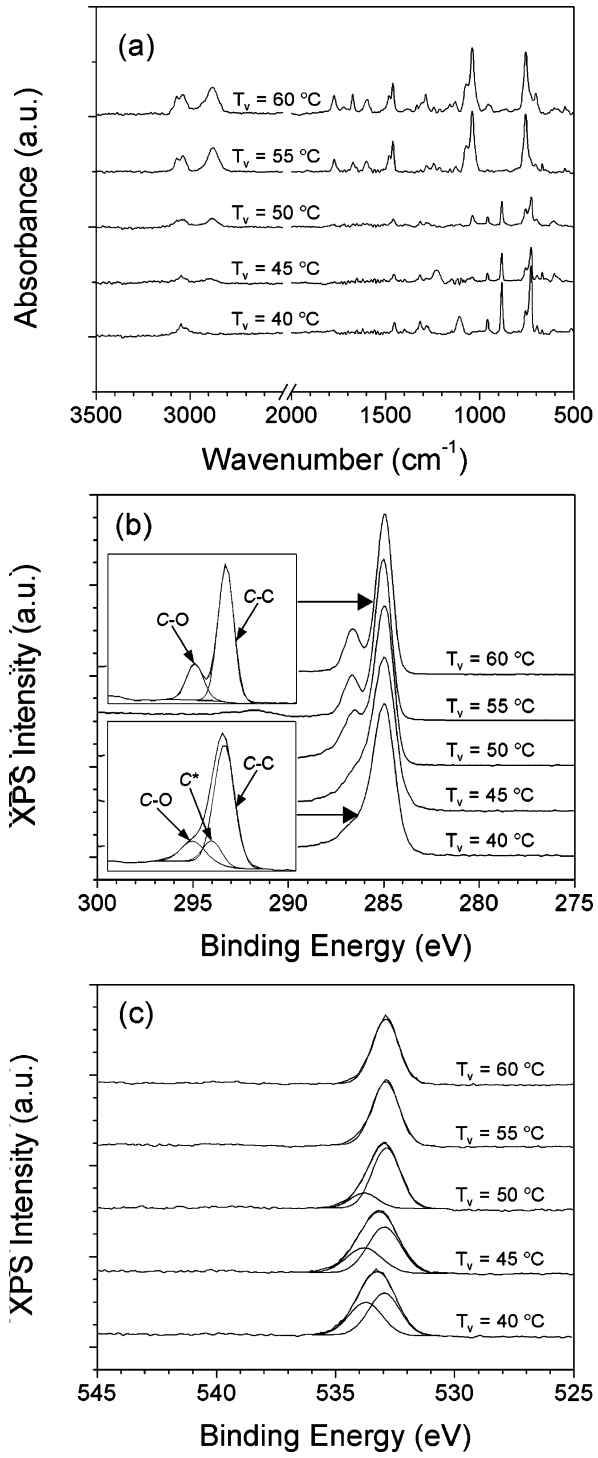

Figure 9. (a) FT-IR spectra of PIBF films prepared at various vaporization temperatures. (b) C(1s) high-resolution XPS spectra of the PIBF films prepared at various vaporization temperatures. The lower inset is a typical example of the curve fitting for three peak components (i.e., *C*−C, **C*, and *C*−O centered at 285.0, 285.7, and 286.7 eV, respectively). (c) O(1s) high-resolution XPS spectra of the PIBF films prepared at various vaporization temperatures. The spectra of $T_v = 50$, 45, and 40 °C can be resolved into two peak components (i.e., C−*O* and **O* centered at 532.9 and 533.8 eV, respectively). Other operating conditions were fixed at $T_s = 10$ °C, $T_p = 750$ °C, and $P = 0.2$ Torr.

supported by the decrease in the molecular weight of PIBF films from 8300 ($T_v = 60$ °C) to 600 ($T_v = 40$ °C) by GPC analyses.

XPS survey scans showed that there is no significant difference in the atomic composition of this series of PIBF films, which are typically 84.8% (C) and 15.2% (O). These values are consistent with those from the other sets of PIBF films and the stoichiometriy of PIBF (85.7% of carbon and 14.3% of oxygen). On the other hand, the C(1s) high-resolution scans revealed that this set of PIBF films have slightly different chemical structures from one another. As shown in Figure 9b, the spectra obtained from PIBF films prepared at $T_v = 60$ and 55 °C exhibit nearly identical features in the C(1s) region as observed in the other sets of PIBF films. Each spectrum consists of two peak components corresponding to the unsaturated carbons (i.e., *C*−C or *C*−H in the benzene ring) and the oxygen-bound carbon (i.e., *C*−O in the furanoid ring), centered at the binding energies of 285.0 and 286.7 eV, respectively. Area fractions of these peak components are typically 75.9% (*C*−C or *C*−H) and 24.1% (*C*−O), in good agreement with the stoichiometry of PIBF (75% of *C*−C and 25% of *C*−O). As the vaporization temperature decreases, we observed that the peak areas of the unsaturated carbon (centered at the binding energy of 285.0 eV) and the oxygen-bound carbon (centered at the binding energy of 286.8 eV) decrease, and a new peak component centered at the binding energy of 285.7 eV appears. This peak component centered at 285.7 eV is usually assigned as a carbon adjacent to either a carboxyl or an ester group (i.e., *C*−C(═O)−OR) when it appears along with their carbonyl peak components centered typically at 288.5−289.3 eV.[23] However, these spectra do not appear to have a carbonyl peak component and can be resolved into three peak components in the C(1s) region, corresponding to *C*−C (285.0 eV), **C* (285.7 eV), and *C*−O (286.8 eV). Inclusion of ketal (acetal) groups in the films could be an alternative explanation for this new peak component, but ketal compounds are not observed in the expected region of higher binding energy, i.e., centered at ∼288.0 eV, in the high-resolution C(1s) spectra. From the high-resolution O(1s) spectra of the polymer films grown under lower vaporization temperatures (50, 45, and 40 °C), we also observed that the O(1s) peaks can be resolved into two peak components (Figure 9c); one corresponds to C−*O* (532.9 eV), which is nearly identical to the single peak component present in the typical PIBF films, and the other is a new peak, **O* (533.8 eV). Since the binding energy of the oxygen atom of the carbonyl group usually appears around 532.3 eV (for an aliphatic compound) or 531.3 eV (for an aromatic compound),[23] this new peak component centered at 533.8 eV cannot be considered to be an oxygen atom from a carbonyl group but could be an oxygen atom bound to a different functional group. We also checked for the presence of a carbonyl component in this set of polymer films through IR analysis, but the carbonyl absorption in the FT-IR spectra of this set of PIBF films could not be resolved because of the overlap of carbonyl and the weak combination/overtone bands for the ortho-substituted as well as the poor signal-to-noise ratio in the carbonyl region (1690−1810 cm^{-1}).

To clarify whether a carbonyl component was present in this set of PIBF films, we performed NMR analysis. The ^{1}H NMR spectrum of the PIBF film prepared at $T_v = 60$ °C exhibited two broad peaks at 4.6−6.0 and 6.2−8.2 ppm, corresponding to the protons from the furanoid ring and the aromatic protons, respectively. On the other hand, the ^{1}H NMR spectrum of the film prepared at $T_v = 45$ °C showed not only two broad peaks at 4.6−6.0 and 6.2−8.2 ppm but also several multiplets in the 7.0−8.6 ppm range, which could correspond to small molecules produced as byproducts. We also performed ^{13}C NMR to look for the presence of carbonyl in the film. We observed no sign of carbonyl carbons, which usually appear between 150 and 220 ppm in ^{13}C NMR, but carbons from the benzene ring and

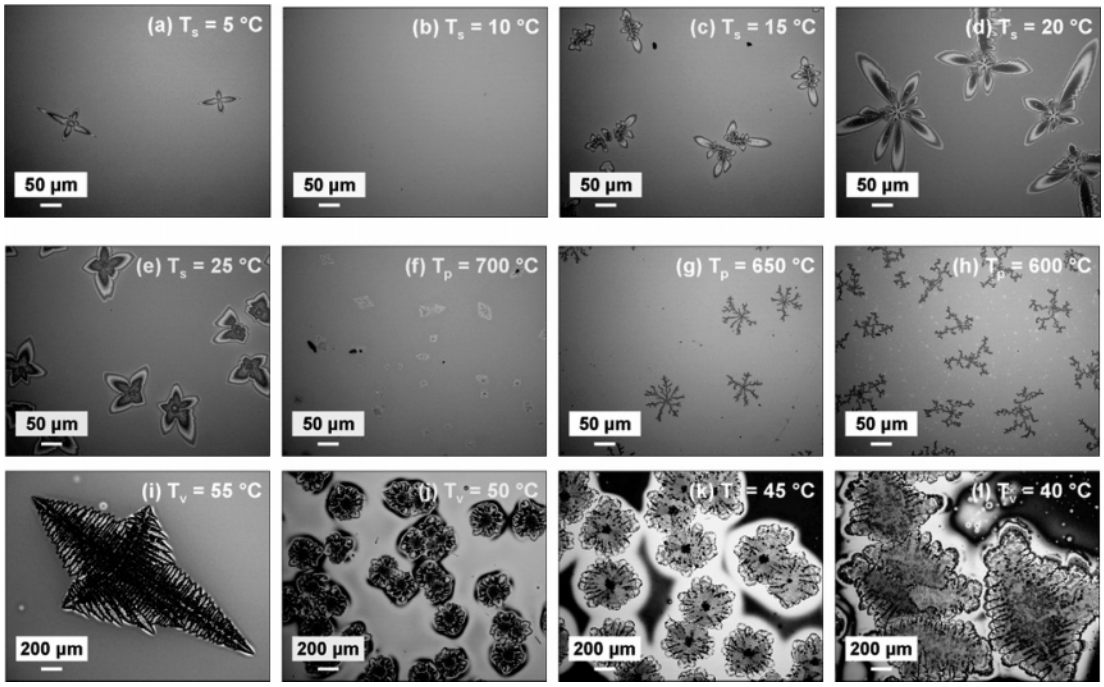

Figure 10. Optical micrographs showing the effects of the stage temperature, the pyrolysis temperature, and the vaporization temperature on the PIBF film morphology: (a−e) stage temperature variation with the fixed T_p = 750 °C and T_v = 60 °C; (f−h) pyrolysis temperature variation with the fixed T_s = 10 °C and T_v = 60 °C; (i−l) vaporization temperature variation with the fixed T_s = 10 °C and T_p = 750 °C. The pressure in the chamber was controlled at 0.2 Torr in all cases.

Table 1. Analyses of the C(1s) and O(1s) High-Resolution XPS Spectra of PIBF Films Prepared under Different Vaporization Temperatures (T_v)

	C(1s) composition (%)			O(1s) composition (%)	
T_v (°C)	*C*−C (BE: 285.0 eV)	*C** (BE: 285.7 eV)	*C*−O (BE: 286.7 eV)	C−*O* (BE: 532.9 eV)	*O** (BE: 533.8 eV)
40	73.8	12.1	14.1	55.4	44.6
45	73.5	10.1	16.4	63.5	36.5
50	73.6	5.6	20.8	80.6	19.4
55	76.2		23.8	100.0	
60	75.9		24.1	100.0	

the furanoid ring (polymer backbone) at 120−140 and 86 ppm, respectively, were apparent.

From these results, we suggest that the peak component centered at 285.7 eV in the high-resolution C(1s) XPS spectra might derive from carbons attached to another type of C−O bond present in the polymerization byproducts. We suspect that ring strain on the furanoid components of the byproducts (with different chemical structures from PIBF) could result in different binding states of the carbons adjacent to the C−O bond in the furanoid ring. Area fractions of these peak components are summarized in Table 1. The generation of small molecules as byproducts in the lower vaporization temperature cases (i.e., T_v = 50, 45, 40 °C) might be due to a longer residence time of the precursor molecule in the pyrolysis zone. The vapor pressure of the precursor molecule decreases as the vaporization temperature decreases, and thereby the flow rate of the precursor molecule becomes slower than that of the higher vaporization temperature, such as T_v = 60 °C. Accordingly, the residence time of the precursor molecule under lower vaporization temperatures becomes longer, and the precursor molecules could obtain excess thermal energy in the pyrolysis zone. Consequently, the excess thermal energy could activate other reaction pathways, which may generate byproducts, such as other cyclic oligomers and decomposed materials.

The thickness of the PIBF films prepared at T_v = 60 and 55 °C are typically about 510 and 400 nm at the center and the edge of the substrate, respectively, similar to those of the PIBF films from the various stage and pyrolysis temperatures. As the vaporization temperature decreases, the film uniformity worsens. This poor uniformity in film thickness over the substrate might be due to large numbers of defects generated in the polymer films through the incorporation of byproducts. By considering the molecular structure, the molecular weight, and the film uniformity, we selected 60 °C as an optimal vaporization temperature for the PIBF film growth.

Surface Morphology of PIBF Films. Figure 10 shows optical microscope images of PIBF films prepared under the various stage, pyrolysis, and vaporization temperatures. Except for the film prepared at T_s = 10 °C, T_p = 750 °C, and T_v = 60 °C (Figure 10b), all films have defects on the surface. The defects in the PIBF film prepared at T_s = 5 °C have four symmetric arms, as shown in Figure 10a. The defects in the PIBF films prepared at T_s = 15 and 20 °C (Figure 10c and d, respectively) have four to eight arms with inhibition of defect growth by a branch developed from the adjacent defect domains. In the PIBF film prepared at T_s = 25 °C (Figure 10e), the defects have four to five arms and are smoother than those present in the PIBF films prepared at T_s = 15 and 20 °C, with the similar inhibition effect on the defect growth. The overall shapes of defects in the PIBF film prepared at T_p = 700 °C (Figure 10f) are similar, but with arms that are broader and smoother than those on the PIBF film prepared at T_s = 5 °C. As the pyrolysis temperature decreases, the defects show a typical fractal branching form similar to a disordered polycrystalline dendrite observed in diffusion-limited aggregation (Figure 10g,h).[24] The difference between the defects in the PIFB films prepared at

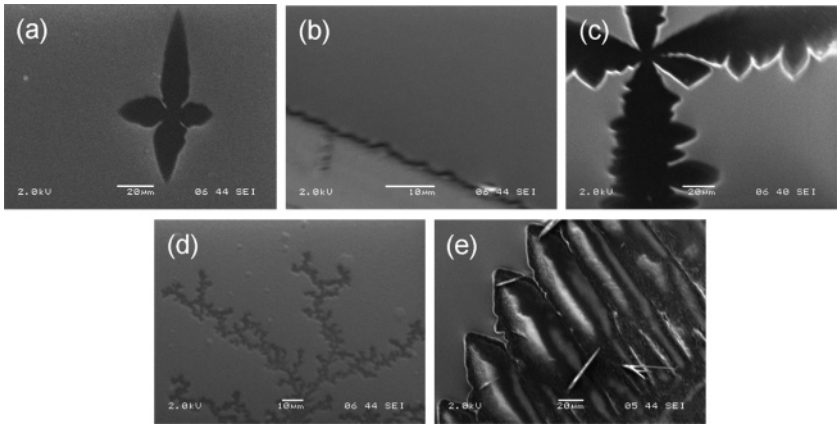

Figure 11. Scanning electron micrographs showing the defects on the PIBF films prepared at (a) $T_s = 5$ °C, $T_p = 750$ °C, and $T_v = 60$ °C; (b) $T_s = 10$ °C, $T_p = 750$ °C, and $T_v = 60$ °C; (c) $T_s = 20$ °C, $T_p = 750$ °C, and $T_v = 60$ °C; (d) $T_s = 10$ °C, $T_p = 650$ °C, and $T_v = 60$ °C; (e) $T_s = 10$ °C, $T_p = 750$ °C, and $T_v = 55$ °C. The pressure in the chamber during the deposition was controlled at 0.2 Torr in all cases. Micrograph b is a cross-section image of the PIBF film on a Si wafer where the lighter part in lower left is the Si wafer and the rest is the PIBF film deposited on the Si wafer.

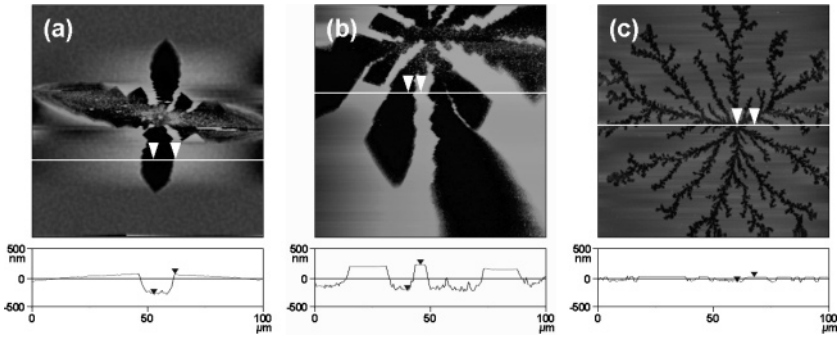

Figure 12. AFM images of the defect domains in the PIBF films. All images obtained by tapping mode with 100 μm × 100 μm of scan size and 1.5 Hz of scan rate. (a) Section analysis of the defect domain of the PIBF film prepared at $T_s = 5$ °C, $T_p = 750$ °C, and $T_v = 60$ °C. The height difference between the top of the PIBF domain and the bottom of the defect domain is 350 nm. (b) Section analysis of the defect domain of the PIBF film prepared at $T_s = 20$ °C, $T_p = 750$ °C, and $T_v = 60$ °C. The height difference is 450 nm. (c) Section analysis of the defect domain of the PIBF film prepared at $T_s = 10$ °C, $T_p = 650$ °C, and $T_v = 60$ °C. The height difference is 85 nm.

650 and 600 °C is the surface density of the defects, ~40/mm^2 for 650 °C and ~70/mm^2 for 600 °C, and the size of the defects, ~50 μm for 650 °C and ~100 μm for 600 °C. The defect in the PIBF film prepared at $T_v = 55$ °C (Figure 10i) shows a typical dendrite, similar to a single-crystalline ordered dendrite with crystallographic symmetry.[24,25] Further decrease in the vaporization temperature leads to morphological changes of defects; disordered dendrite morphologies appear, and the size of the defects increases as the vaporization temperature decreases (Figure 10j−l).

By scanning electron microscopy (SEM), we found that all these defects appear to be hollowed into the polymer films (Figure 11). Figure 11e shows the typical morphology of directional growth of the defect, which is very similar to the directional dendritic growth during the crystallization of ice in sucrose solution.[26] To further elucidate the surface morphology of the PIBF domains and the defect domains, we performed surface analysis by AFM. From the section analysis, we found that the height difference between the top of PIBF domain and the bottom of the defect domain is typically 350 and 450 nm in the film prepared at $T_s = 5$ °C (Figure 12a) and $T_s = 20$ °C (Figure 12b), respectively. In the film prepared at $T_p = 650$ °C, the height difference between two domains is 85 nm, as shown in Figure 12c. These results suggest that the nonequilibrium conditions developed at the interface between the PIBF domain and the defect domain could induce the inhibition of the PIBF growth at the interface by interfering with the initiation and the propagation of polymerization. This interference in both initiation and propagation of polymerization would occur when the monomer (IBF) for the polymerization is not available at this interface. The unavailability of IBF monomer can be attributed to either poor adsorption of the monomer on this region or deactivation of monomer to form unpolymerizable compounds.[27] Because the growth of polymer eventually occurs on both PIBF and defect domains, the deactivation of the monomer is more likely, rendering it unavailable for the initiation and the propagation of polymerization. This effect could lead to a different growth rate of the defect domain from that of the PIBF domain, as evidenced by the section analysis across these two domains (Figure 12).

The defects might be derived from various sources, including deactivated forms of IBF, unpyrolyzed precursor monomers, oligomeric byproducts, or decomposed materials, which would not be able to polymerize to form PIBF. For the convenience of the following discussion, we denote polymerizable IBF monomers as the active species, whereas unpolymerizable compounds mentioned above are referred to as the unreactive species. Assuming that the domains first occupied by the active species are a continuous phase (i.e., large numbers of nucleation sites or propagation centers for polymerization are distributed over the entire surface) and the others occupied by the unreactive species are a dispersed phase (i.e., small numbers of sites occupied by the unreactive species are present among the polymer nucleation sites), the defect growth in the PIBF film

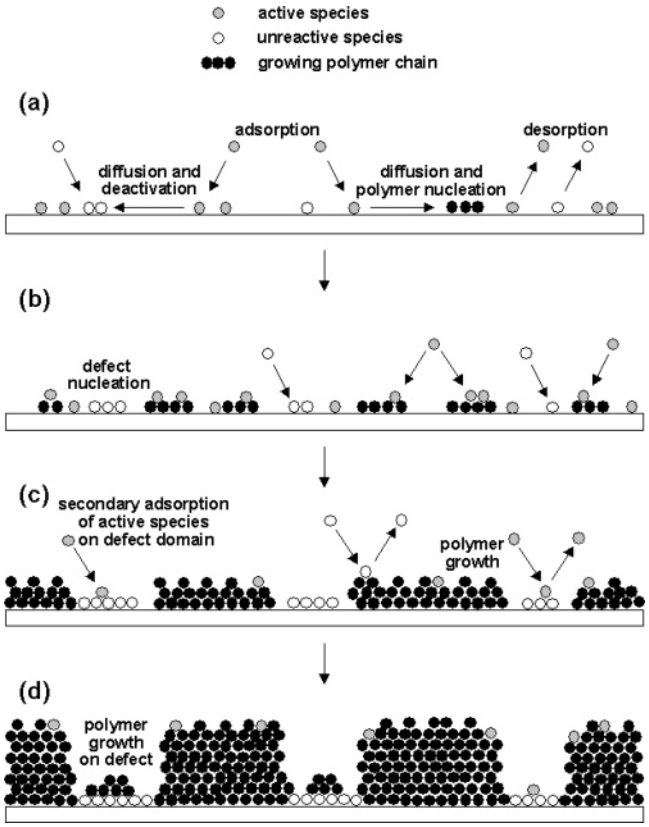

Figure 13. Schematic illustration of PIBF growth and defect formation. (a) Polymer nucleation: There is competition among adsorption, diffusion, deactivation, and desorption processes. Polymer nucleation and surface growth of PIBF start at the sites occupied by the active species. (b) Propagation of polymer and nucleation of defects: Surface growth of PIBF proceeds with adsorption of additional active species. Accumulation of the unreactive species leads to nucleation of the defect domain. (c) Polymer growth and secondary adsorption of active species onto the defect domain: The localization of the active species on the growing polymer chains results in a rapid growth of the polymer in the PIBF domain. The secondary adsorption of the active species occurs in the defect domain; these parts can develop into the formation of nucleation sites for polymerization. (d) The different growth rates resulting from the nonequilibrium conditions at the interface between the PIBF domain and the defect domain lead to the height difference between two domains and the generation of the various shapes of the defects.

can be considered as the nonequilibrium growth, which is usually observed in crystal growth under nonequilibrium conditions[28] or domain formation in Langmuir monolayers of fatty acids during the phase transition from expanded phase to condensed phase.[29]

As illustrated in Figure 13, the initial step of PIBF film growth would be the adsorption of the active species onto the surface to initiate and propagate the polymerization. We suspect that the sites first occupied by the unreactive species would develop into nuclei for defect formation,[30] which induce the deactivation of the adsorbing active species and generate an energetically unfavorable surface for initiation and propagation of polymerization. When the active species reach the surface, some of these active species diffuse laterally along the surface and irreversibly adsorb onto the surface and initiate polymerization, whereas others would desorb from the surface or become an unreactive species by a deactivation process induced through interaction with other irreversibly adsorbed unreactive species. Once polymer nucleation occurs on the surface, propagation of polymerization commences, and polymer growth proceeds in a normal fashion when supplied with fresh active species.

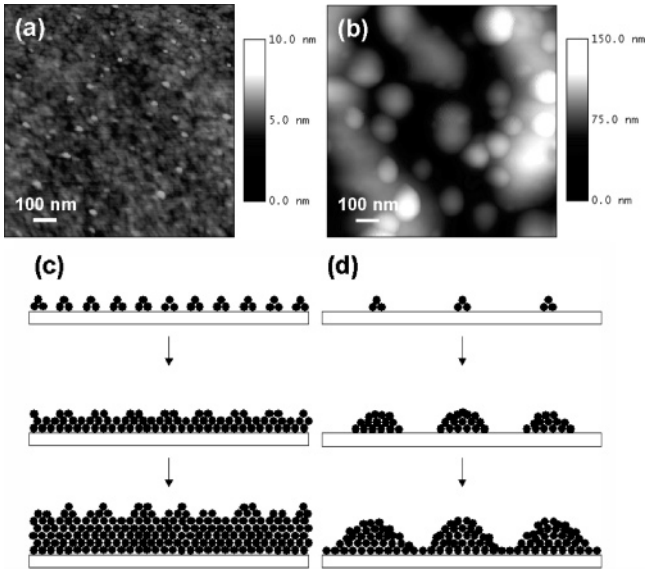

Figure 14. Typical topographies of (a) a PIBF domain and (b) a defect domain (scan size and scan rate are 1 μm $\times$ 1 μm and 1.5 Hz, respectively, for both cases) and their corresponding schematics for polymer growth with (c) multiple nucleation sites for polymerization in the PIBF domain and (d) fewer nucleation sites for polymerization in the defect domain.

Meanwhile, the accumulation of the unreactive species develops into nuclei for defect formation. The nuclei for the defects would favor the adsorption of unreactive species and/or deactivation of adsorbing active species; this behavior leads to the inhibition of polymer growth in the defect domain. However, if the delivery rate of the active species is high enough to overcome the deactivation rate of adsorbing active species, there might be a possibility for secondary adsorption of active species onto the defect domain. The secondary adsorption could induce polymer nucleation on the defect domain although the process would be less efficient than in the PIBF domain. Since this process is unfavorable, fewer nucleation sites for polymer growth would be expected in the defect domain than in the PIBF domain, and the polymer growth in the defect domain would become slower than that in the PIBF domain. Consequently, this process could explain the height difference between two domains and the generation of the various patterns of the defect domains.

The surface morphologies of the PIBF and the defect domains are additional evidence that supports the inhibition of polymer growth in the defect domain.[32] Figure 14a shows the topography of the typical PIBF domain with an average rms roughness of 1.6 nm. We observed that small grains with the average size of 35 nm are uniformly distributed over the entire surface of the PIBF domain, whereas the defect domain has a rougher surface with an average rms roughness of 22.8 nm (Figure 14b) and much bigger sized grains up to 350 nm, mixed with small grains in the defect domain. The uniformly distributed small grains in PIBF domain suggest that multiple nucleation sites for polymerization (i.e., propagation center) would exist on the surface, which form a large number of small polymer grains that coalesce into a continuous layer (Figure 14c). On the other hand, nonuniformly distributed large grains in the defect domain indicate that there are fewer nucleation sites for polymerization and the polymerization process is starved for active species on the surface, which results in the formation of fewer grains growing to larger sizes before coalescence (Figure 14d).[33]

Cationic Initiation of IBF Polymerization. To investigate the possible role of cationic initiation of IBF polymerization in

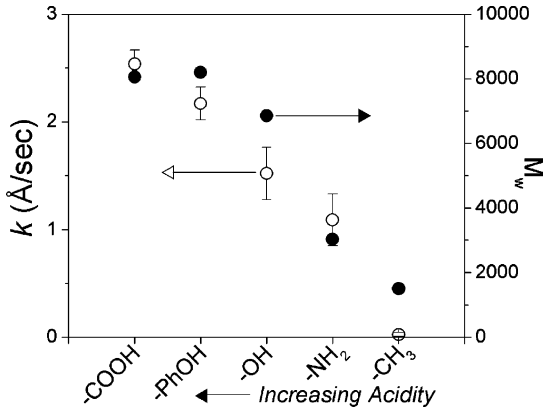

Figure 15. Growth rate (○) and weight-average molecular weight (●) of polymer films deposited on the surfaces with functional groups of different acidity: −COOH, −PhOH, −OH, $-NH_2$, and $-CH_3$. The growth rate and the weight-average molecular weight of PIBF films decreased with the decrease in acidity of the surface functional groups.

Scheme 2. A Possible Cationic Initiation of IBF Polymerization

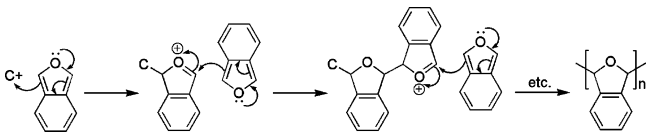

the CVD process (Scheme 2), we deposited PIBF on several surfaces tailored with functional groups of different acidities, including a carboxylic acid (−COOH), a phenol (−PhOH), an alcohol (−OH), an amine ($-NH_2$), and a methyl group ($-CH_3$). We observed the fastest growth of PIBF ($k = 2.5$ Å/s) on the carboxylic acid-terminated surfaces while PIBF films grew very slowly on the methyl-terminated surfaces ($k = 0.02$ Å/s). In general, the growth rate of the PIBF films decreased with the decrease in acidity of the surface functional group (Figure 15). In addition, GPC analysis of this set of polymer films revealed that the weight-average molecular weights of PIBF grown on carboxylic acid- and phenol-terminated surfaces were around 8000 and decreased to 1500 as the acidity of the surface functional group decreased (Figure 15). The FT-IR analysis on this set of films indicated that the films grown on carboxylic acid-, phenol-, and alcohol-terminated surfaces appear to have nearly identical spectra to those obtained from the typical PIBF films, whereas the spectra of the films grown on amine- and methyl-terminated surfaces are similar to those of the dendritic (or disordered dendritic) defect-containing films prepared at lower vaporization temperatures, such as $T_v = 50$, 45, and 40 °C (data not shown). The XPS analysis on this set of films also revealed that the C(1s) high-resolution spectra of PIBF films grown on the carboxylic acid-, phenol-, and alcohol-terminated surfaces appear to have two peak components (*C*−C and *C*−O centered at 285.0 and 286.7 eV, respectively) with similar area fractions to those of the typical PIBF films while the spectra of the films grown on amine- and methyl-terminated surfaces are resolved into three peak components (i.e., *C*−C, **C*, and *C*−O centered at 285.0, 285.7, and 286.7 eV, respectively) that are similarly observed in those of the films prepared at lower vaporization temperatures (data not shown). By optical microscopy, we observed that the films grown on carboxylic acid-, phenol-, and alcohol-terminated surfaces are defect-free, whereas disordered dendritic defects and discontinuous growth (i.e., islandlike growth) appear in the films grown on the amine-terminated surfaces and methyl-terminated surfaces, respectively (data not shown). We also investigated the possibility of radical initiation of IBF polymerization by depositing PIBF film with *tert*-butyl peroxide (TBPO) as an initiator. We observed no significant changes in growth rate ($k \sim 2.3$ Å/s), chemical structure (similar characteristic absorption bands in FT-IR spectra), and chemical composition (76.2% and 23.8% for *C*−C and *C*−O in high-resolution C(1s) XPS spectra, respectively) from the films grown with TBPO. All these kinetic, spectroscopic, and microscopic results suggest that the growth of PIBF follows a surface cationic polymerization mechanism rather than a radical polymerization.

Conclusions

We synthesized poly(isobenzofuran) (PIBF) films from 1,2,3,4-tetrahydro-1,4-epoxynaphthalene as a precursor monomer by a thermal chemical vapor deposition (CVD) process. The deposition temperature, pyrolysis temperature, and vaporization temperature strongly affected chemical structure, growth rate, molecular weight, and morphology of the PIBF films. Optimization of the operating conditions provided a useful protocol to obtain a defect-free coating of PIBF. Using the optimal conditions ($T_s = 10$ °C, $T_p = 750$ °C, $T_v = 60$ °C, and $P = 0.2$ Torr), we obtained uniform polymer films with 2.3 Å/s of growth rate. Structural retention of the PIBF films prepared by the thermal CVD process was verified by the FT-IR and the XPS analyses. Defects in the polymer films can be derived from various unreactive species that provide an unfavorable environment for the growth of PIBF. The growth of PIBF is very sensitive to the surface properties, specifically the acidity of the surface functional group. Carboxylic acid-terminated surfaces exhibited the fastest growth of PIBF films (2.5 Å/s) while nonacidic surfaces, such as amine- and methyl-terminated ones, have a tendency of inhibition of PIBF growth (0.02 Å/s for methyl-terminated surfaces) and thereby produce defects in the films. Evaluation of PIBF growth on several surfaces tailored with functional groups of differing acidity as well as the lack of effect on PIBF growth by free radical initiation suggests that the polymerization of IBF follows a cationic polymerization mechanism. Studies of defect formation also support that the PIBF growth follows a surface growth mechanism.

The described CVD process enables the reactive IBF monomer to be coated as high-quality polymer thin films that cannot be realized by any solvent-based techniques. Furthermore, this CVD process can be extended to produce various derivatives of functional coatings of PIBF by using specifically substituted precursor monomers. The optical property (refractive index, $n = 1.63$) and surface-dependent growth characteristics of PIBF can provide potential applications, such as a component of optical waveguides and a micropatterning process for polymeric thin films. Current efforts target the development of functional PIBF coatings using substituted precursor monomers for optical and microfluidic applications.

Acknowledgment. This work was supported by the U.S. Army through the Institute for Soldier Nanotechnologies (ISN), under the contract (DAAD-19-02-0002) with the U.S. Army Research Office and in part by the MRSEC program of the National Science Foundation under the award DMR 02-13282. T.M.S. acknowledges support from the Office of Naval Research MURI program. We thank Mr. Saif Khan for help with SEM and Prof. Karen K. Gleason's group at MIT for allowing us to use the GPC and the VASE.

References and Notes

(1) (a) Majid, N.; Dabral, S.; McDonald, J. F. *J. Electron. Mater.* **1988**, *18*, 301. (b) Senkevich, J. J.; Desu, S. B. *Thin Solid Films* **1998**, *322*,

148. (c) Senkevich, J. J.; Mitchell, C. J.; Vijayaraghavan, A.; Barnat, E. V.; McDonald, J. F.; Lu, T.-M. *J. Vac. Sci. Technol. A* **2002**, *20*, 1445.
(2) You, L.; Yang, G. R.; Lang, C. I.; Wu, P.; Moore, J. A.; McDonald, J. F.; Lu, T. M. *J. Vac. Sci. Technol. A* **1993**, *11*, 3047.
(3) Nichols, M. F. *Crit. Rev. Biomed. Eng.* **1994**, *22*, 39.
(4) (a) Burns, M. A.; Johnson, B. N.; Brahmasandra, S. N.; Handique, K.; Webster, J. R.; Krishnan, M.; Sammarco, T. S.; Man, P. M.; Jones, D.; Heldsinger, D.; Mastrangelo, C. H.; Burke, D. T. S*cience* **1998**, *282*, 484. (b) Yang, X.; Grosjean, C.; Tai, Y.-C. Solid-State Sensor and Actuator Workshop, Hilton Head Island, SC, June 8−11, 1998, p 316.
(5) Gaynor, J.; Desu, S. B. *J. Mater. Res.* **1994**, *9*, 3125.
(6) Vaeth, K. M.; Jackman, R. J.; Black, A. J.; Whitesides, G. M.; Jensen, K. F. *Langmuir* **2000**, *16*, 8495.
(7) (a) Lahann, J.; Balcells, M.; Rodon, T.; Lee, J.; Choi, I. S.; Jensen, K. F.; Langer, R. *Langmuir* **2002**, *18*, 3632. (b) Lahann, J.; Langer, R. *Macromolecules* **2002**, *35*, 4380. (c) Lahann, J.; Balcells, M.; Lu, H.; Rodon, T.; Jensen, K. F.; Langer, R. *Anal. Chem.* **2003**, *75*, 2117. (d) Suh, K. Y.; Langer, R.; Lahann, J. *Adv. Mater.* **2004**, *16*, 1401.
(8) (a) Leezenberg, P. B.; Reiley, T. C.; Tyndall, G. W. *J. Vac. Sci. Technol. A* **1999**, *17*, 275. (b) Butoi, C. I.; Mackie, N. M.; Barnd, J. L.; Fisher, E. R.; Gamble, L. J.; Castner, D. G. *Chem. Mater.* **1999**, *11*, 862. (c) Butoi, C. I.; Mackie, N. M.; Gamble, L. J.; Castner, D. G.; Miller, A. M.; Barnd, J. L.; Fisher, E. R. *Chem. Mater.* **2000**, *12*, 2014. (d) Lau, K. K. S.; Caulfield, J. A.; Gleason, K. K. *Chem. Mater.* **2000**, *12*, 3032. (e) Murthy, S. K.; Gleason, K. K. *Macromolecules* **2002**, *35*, 1967. (f) Lau, K. K. S.; Bico, J.; Teo, K. B. K.; Chhowalla, M.; Amaratunga, G. A. J.; Milne, W. I.; McKinley, G. H.; Gleason, K. K. *Nano Lett.* **2003**, *3*, 1701. (g) Biloiu, C.; Biloiu, I. A.; Sakai, Y.; Sugawara, H.; Ohta, A. *J. Vac. Sci. Technol. A* **2004**, *22*, 1158.
(9) (a) Vaeth, K. M.; Jensen, K. F. *Adv. Mater.* **1999**, *11*, 814. (b) Vaeth, K. M.; Jensen, K. F. *Macromolecules* **2000**, *33*, 5336.
(10) (a) Ryan, M. E.; Hynes, A. M.; Wheale, S. H.; Badyal, J. P. S.; Hardacre, C.; Ormerod, R. M. *Chem. Mater.* **1996**, *8*, 916. (b) Groenewoud, L. M. H.; Engbers, G. H. M.; Terlingen, J. G. A.; Wormeester, H.; Feijen, J. *Langmuir* **2000**, *16*, 6278. (c) Martin, L.; Esteve, J.; Borrós, S. *Thin Solid Films* **2004**, *451*−*452*, 74.
(11) Lee, H. J.; Kim, D. S.; Suh, M. C.; Shim, S. C. *J. Polym. Sci., Part A* **1996**, *34*, 3255.
(12) (a) Popat, K. C.; Johnson, R. W.; Desai, T. A. *J. Vac. Sci. Technol. B* **2003**, *21*, 645. (b) Murthy, S. K.; Olsen, B. D.; Gleason, K. K. *Langmuir* **2004**, *20*, 4774.
(13) (a) Haddadin, M. J. *Heterocycles* **1978**, *9*, 865. (b) Rodrigo, R. *Tetrahedron* **1988**, *44*, 2093.
(14) Fieser, L. F.; Haddadin, M. J. *J. Am. Chem. Soc.* **1964**, *86*, 2081.
(15) Warrener, R. N. *J. Am. Chem. Soc.* **1971**, *93*, 2346.
(16) Wiersum, U. E.; Mijs, W. J. *J. Chem. Soc., Chem. Commun.* **1972**, 347.
(17) (a) Fieser, L. F.; Haddadin, M. J. *Can. J. Chem.* **1965**, *43*, 1599. (b) Wittig, G.; Pohmer, L. *Chem. Ber.* **1956**, *89*, 1334.
(18) (a) Mao, Y.; Gleason, K. K. *Langmuir* **2004**, *20*, 2484. (b) Chan, K.; Gleason, K. K. *Langmuir* **2005**, *21*, 8930.
(19) Lau, K. K. S.; Caulfield, J. A.; Gleason, K. K. *J. Vac. Sci. Technol. A* **2000**, *18*, 2404.
(20) Pavia, D. L.; Lampman, G. M.; Kriz, G. S. *Introduction to Spectroscopy*, 2nd ed.; Saunders College Publishing: New York, 1996; Chapter 2.
(21) Besides the thickness information, we obtained optical properties through VASE analysis on PIBF films. For this set of PIBF films, the average values of refractive index (n) and extinction coefficient (k_e) were 1.63 (standard deviation of 0.07) and 0.0042 (standard deviation of 0.0007), respectively. Since the square of the refractive index of the material equals the optical dielectric constant (the lower bound to the actual dielectric constant) of the material,[19] we obtained the optical dielectric constant using the refractive index of each film; the average is 2.67 with a standard variation of 0.05.
(22) Further increases in the pyrolysis temperature (i.e., $T_p = 800$ and 850 °C) resulted in the formation of the different shapes of defects (i.e., disordered dendrites), the decrease in the molecular weight ($M_w \sim 600$ at $T_p = 850$ °C), and significant differences in the chemical structures/composition of the films, which were similarly observed from the films prepared at lower vaporization temperature (i.e., $T_v \leq 50$ °C). These results suggest that higher pyrolysis temperatures produce different materials, such as decomposed materials or non-polymerizable compounds, by excess thermal energy provided in the pyrolysis zone, as described in the next section (vaporization temperature dependence of the PIBF film growth).
(23) Beamson, G.; Griggs, D. *High-Resolution XPS of Organic Polymers: The Scienta ESCA300 Database*; John Wiley & Sons: New York, 1992; pp 277−292.
(24) (a) Witten, T. A.; Sander, L. M. *Phys. Rev. Lett.* **1981**, *47*, 1400. (b) Meakin, P. *Phys. Rev. A* **1983**, *27*, 604. (c) Sander, L. M. *Nature (London)* **1986**, *322*, 789. (d) Oaki, Y.; Imai, H. *Cryst. Growth Des.* **2003**, *3*, 711.
(25) Tian, Z. R.; Liu, J.; Voigt, J. A.; Xu, H.; Mcdermott, M. J. *Nano Lett.* **2003**, *3*, 89.
(26) Butler, M. F. *Cryst. Growth Des.* **2001**, *1*, 213.
(27) We speculate that the possible structures of deactivated IBF could include oligomeric forms, such as other dimers, other cyclic oligomers, or some decomposition product.
(28) (a) Langer, J. S. *Science* **1989**, *243*, 1150. (b) Ben-Jacob, E.; Garik, P. *Nature (London)* **1990**, *343*, 523.
(29) (a) Miller, A.; Knoll, W.; Möhwald, H. *Phys. Rev. Lett.* **1986**, *56*, 2633. (b) Knobler, C. M. *Science* **1990**, *249*, 870. (c) McConnell, H. M. *Annu. Rev. Phys. Chem.* **1991**, *42*, 171. (d) Heron, S.; Meunier, J. *J. Chem. Phys.* **1993**, *98*, 9148. (e) Gehlert, U.; Vollhardt, D. *Langmuir* **1997**, *13*, 277. (f) Weidemann, G.; Vollhardt, D. *Langmuir* **1997**, *13*, 1623 (g) Iimura, K.; Yamauchi, Y.; Tsuchiya, Y.; Kato, T. *Langmuir* **2001**, *17*, 4602.
(30) The formation of defects might also be due to stress development resulting from the interaction among the polymer chains during the polymerization. To clarify the possible contribution of stress to the defect formation, we also measured the stress on the PIBF films with Tencor FLX-2320 stress gauge. The equation used to determine the stress is the Stoney formula,[31] in which the stress is dependent on several variables, such as the thickness of the substrate and the film, substrate modulus (125 GPa for Si wafer), substrate Poisson's ratio (0.27 for Si wafer), and the change in the curvature of the substrate before and after the film deposition, etc. Overall, we observed that there is little, essentially zero, stress, ranging from 10^{-4} to 10^{-5} GPa, in our films whether they contain defects or not. It is possible that the stress built up in the films would be relieved during the deposition process so that we only could obtain very low (essentially zero) stress values. From these results, we conclude that the defect formation and growth is mainly due to the adsorption and accumulation of unreactive species although there could be small contribution from the stress.
(31) (a) Stoney, G. G. *Proc. R. Soc. London, Ser. A* **1909**, *82*, 172. (b) Freund, L. B.; Floro, J. A.; Chason, E. *Appl. Phys. Lett.* **1999**, *74*, 1987. (c) Chen, K.-S.; Ou, K.-S. *J. Micromech. Microeng.* **2002**, *12*, 917.
(32) Vaeth, K. M.; Jensen, K. F. *Chem. Mater.* **2000**, *12*, 1305.
(33) In the GPC analysis, every PIBF film showed a minor peak corresponding to the weight-average molecular weight of 370000−500000 with area fractions ranging from 1 to 10%. These results support that the defect domains would have fewer nucleation sites for polymerization, and the polymers would grow to have longer chains.

MA060345N